Quantum oscillations in type-II Dirac semimetal $PtTe_2$

Dongzhi Fu,[1] Xiangyan Bo,[1] Fucong Fei,[1] Bin Wu,[1] Ming Gao,[2] Xuefeng Wang,[2] Muhammad Naveed,[1] Syed Adil Shah,[1] Haijun Bu,[1] Baigeng Wang,[1] Lu Cao,[1,*] Wenqin Zou,[1,*] Xiangang Wan,[1] and Fengqi Song[1,*]

[1]*National Laboratory of Solid State Microstructures, Collaborative Innovation Center of Advanced Microstructures, and College of Physics, Nanjing University, Nanjing 210093, P. R. China*

[2]*National Laboratory of Solid State Microstructures, Collaborative Innovation Center of Advanced Microstructures, and School of Electronic Science and Engineering, Nanjing University, Nanjing 210093, P. R. China*

(Received 9 February 2018; published 7 June 2018)

Type-II Dirac semimetal (DSM) phase, in which Lorentz invariance is broken, has been experimentally realized in $PtSe_2$ class. We study the transport properties and Fermi surface (FS) morphology of $PtTe_2$ by de Haas–van Alphen (dHvA) quantum oscillations. Quantum oscillations analyses for out-of-plane and in-plane magnetizations revealed multiple frequencies with low effective mass and high quantum mobility. First-principles calculations are performed to confirm the existence of type-II Dirac fermions in $PtTe_2$ and distinguish the contributing pockets for each oscillation mode. Among all the observed frequencies, one around 4510 T is identified to be derived from the electron pocket that participates in the formation of the type-II Dirac cone.

DOI: 10.1103/PhysRevB.97.245109

I. INTRODUCTION

Though Dirac and Weyl fermions were initially proposed in high-energy physics [1], Weyl fermions have never been discovered experimentally as elementary particles. In recent years, their counterpart (low-energy excitations) in condensed matter physics have been implemented, which has ignited explosive research on three-dimensional (3D) topological semimetals [2–8]. 3D DSMs were first realized in Na_3Bi [9,10] and Cd_3-As_2 [11,12] with quadruple degenerate linear band crossings (Dirac points) appearing near the Fermi level. If the inversion symmetry or time-reversal symmetry is broken, a spin-degenerate Dirac fermion will evolve into two Weyl fermions with opposite chirality [2,3,13]. 3D Weyl semimetals (WSMs) were realized in the TaAs family [2,3] and feature open Fermi arcs as topological surface states. Due to the linear dispersion near the crossing, Dirac and Weyl fermions can be described by massless Dirac and Weyl equations, respectively. In 3D DSMs or WSMs, the existence of Dirac or Weyl fermion in the vicinity of the Fermi level gives rise to a variety of exotic physical properties, such as negative magnetoresistance induced by chiral anomaly [14,15] and quantum oscillations arising from Fermi arcs [16,17].

Lorentz invariance is a strict restriction in high-energy physics, however it is not necessary in condensed matter physics. The type-II WSMs that break the Lorentz invariance are predicted and experimentally confirmed in WTe_2 [18,19], $MoTe_2$ [20,21], $Mo_xW_{1-x}Te_2$ [22,23], and LaAlGe [24]. Different from the type-I WSMs with pointlike FS, type-II WSMs have finite FS, forming heavily tilted Weyl cones at the points where electron and hole pockets contact each other [18]. Because of its unique band structure, type-II WSMs have many unique properties that differ from the type-I WSMs: field-selective chiral anomaly [25], intrinsic anomalous Hall effect [26], and momentum space Klein tunneling [27]. Recently, another kind of topological material that violates the Lorentz invariance, the type-II DSMs, has attracted a great deal of research [28–31]. The $PtSe_2$ [28] and $VA1_3$ [32] family are predicted to be type-II DSMs by theoretical calculation. Tilted Dirac cones along the k_z direction were verified by ARPES experiments in most of the members of the $PtSe_2$ class [29,30,33]. In addition, a topological nontrivial quantum oscillation mode is observed in $PdTe_2$ [31], which may be related to the Dirac fermions. However, the transport properties of $PtTe_2$ are not reported yet, and the relevant research urgently needs to be expanded.

Here we study the magnetic transport of $PtTe_2$ by dHvA quantum oscillations. Multiple frequencies are extracted from the analysis of isothermal magnetization in low temperature and high field. We obtained all important transport parameters such as Dingle temperature and quantum mobility by multi-band LK fit. First-principles calculations were conducted to identify the contributing pockets of oscillations frequencies and assist the understanding of band structure of $PtTe_2$.

II. EXPERIMENTAL DETAILS

A high quality single crystal of $PtTe_2$ was grown via self-flux methods. The mixture of Pt and Te with the molar ratio 1:49 was sealed in a quartz tube, which was sealed under vacuum. The quartz tube was heated in a furnace at 800 °C for 48 h to melt and homogenize the starting materials. The furnace was then slowly cooled to 495 °C after 2 weeks to crystallize $PtTe_2$ in Te flux. A single crystal with regular shapes of $PtTe_2$ was obtained via centrifugation after 3 days. The isothermal magnetization measurements were performed with a vibrating sample magnetometer (VSM) oven option in 14 T DynaCool (Quantum Design). The magnetotransport

*Corresponding authors: caolu@nju.edu.cn; wqzou@nju.edu.cn; songfengqi@nju.edu.cn

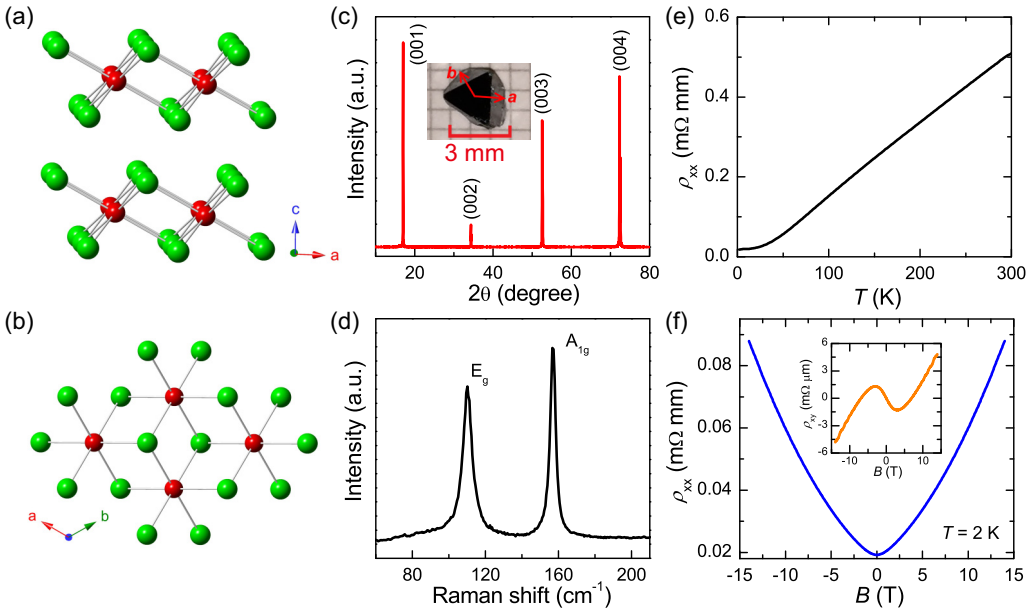

FIG. 1. Crystal structure and characterization of $PtTe_2$. (a) and (b) Side and top views of the crystal structure of $PtTe_2$. Green balls are Te atoms, and red balls are Pt atoms. (c) X-ray diffraction pattern of $PtTe_2$ measured at room temperature. A image of the few-millimeter-size single crystal is shown in the inset, and the directions of a and b are labeled on the sample. (d) Raman spectrum of $PtTe_2$ measured at room temperature. (e) Temperature dependent resistivity of $PtTe_2$. (f) The magnetic-field dependent resistivity up to 14 T at 2 K, with a magnetic field applied along the c-axis direction. The inset shows magnetic field dependence of the Hall resistivity.

measurements, including resistance and Hall effect measurements, were performed using a standard Hall-bar geometry in DynaCool.

III. RESULTS AND DISCUSSIONS

$PtTe_2$ has a centrosymmetric CdI_2-type structure that satisfies the space group $P\bar{3}m1$ and point group $D_{3d}(-3m)$. The adjacent Te atomic layers are connected by weak van der Waals interactions, which make $PtTe_2$ a quasi-two-dimensional layered material. The side and top views of the $PtTe_2$ crystal structure are shown in Figs. 1(a) and 1(b). Figure 1(c) shows the x-ray diffraction pattern of the $PtTe_2$ single crystal. Only the sharp $(00n)$ peaks are observed and no impurity peaks appear, which imply the high quality of the single crystal. The inset of Fig. 1(c) is a typical $PtTe_2$ single crystal with several-millimeter size. The Raman spectrum in Fig. 1(d) shows the E_g and A_{1g} modes at 110 and 157 cm^{-1}, respectively. The E_g and A_{1g} modes correspond to the in-plane oscillations and out-of-plane vibration of the Te atoms, respectively, which are typical features of the 1 T structure [34]. Figure 1(e) shows the temperature-dependent longitudinal resistivity of $PtTe_2$, and the resistivity decreases with decreasing temperature, exhibiting a metallic behavior with a residual resistance ratio about 28. Figure 1(f) is the field dependent resistivity of the sample measured at 2 K, which shows a classic parabolic behavior. The inset is the Hall resistivity of the sample at 2 K and its nonlinearity implies the multiband transport with contributions from different pockets near the FS.

In order to understand the electronic structure of $PtTe_2$ and to explore the origin of its quantum oscillation modes, we have performed first-principles band structure calculations. Bulk Brillouin zone (BZ) is shown in Fig. 2(a) with the high-symmetry points, lines, and Dirac points (D) being indicated. Figures 2(d) and 2(e) is the band dispersion with SOC along the high-symmetry lines (the in-plane S-D-T and out-of-plane A-D-Γ directions). There are remarkable band crossings in the vicinity of D along both the S-D-T and A-D-Γ lines below the Fermi level. Because of belonging to different irreducible representations (2D Δ_4 and 1D Δ_{5+6}, respectively), the two valence bands intersect each other without opening a gap [28]. It is noteworthy that the Dirac cone inclines strongly along k_z direction (Γ-A) but keeps upright along k_x-k_y plane (S-D-T), which is the typical characteristic of a type-II Dirac cone. According to our calculations, the Dirac points reside at 0.82 eV below the Fermi energy at the D point $(0, 0, \pm 0.37)\,2\pi/c$, where c is the lattice constant along z direction.

We have calculated the 3D FS of bulk $PtTe_2$ to compare the calculations and quantum oscillation modes. Figures 2(b) and 2(c) are the top view and side view of the 3D FS, respectively. The FS consists of one apple-core-like hole pocket α in the center of BZ, one flowerlike electron pocket β_1 encompassing the hole pocket, six double-triangular-pyramid-like electron pockets γ located around the K points of the first BZ, and a dozen of fingerlike electron pockets β_2. The electron pockets γ are wrapped by the flowerlike electron pocket, so they cannot be observed in Fig. 2(b). Both the hole and electron pockets have threefold rotation and inversion symmetry, which is consistent with the symmetry of the crystal structure. The apple-core-like hole pocket α and flowerlike electron pocket β_1 have been observed by ARPES experiments [29]. Since the pockets are sensitive to the position of Fermi level, with the Fermi level shifting from the Dirac point to the current location as indicated in Figs. 2(d) and 2(e), the initial electron pocket participating in the forming of the type-II Dirac cone evolves into the current hole pocket α and the initial hole pocket

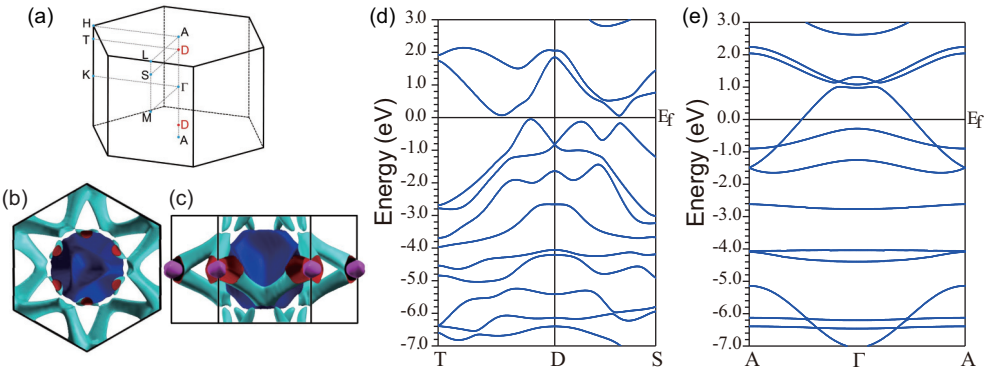

FIG. 2. (a) BZ of bulk with the high-symmetry points being indicated. 3D Dirac point is highlighted by D. (b) the top and (c) side views of the FS in BZ. The aqua green and purple one correspond to electron pockets, and the blue one is hole pocket. (d) The band structure along high symmetry lines in-plane S-D-T direction. (e) The band structure along high symmetry lines out-of-plane A-D-Γ direction.

disappears. Meanwhile, the other electron pockets in Figs. 2(b) and 2(c) arise. Therefore, in Figs. 2(b) and 2(c) only the current hole pocket contributes to the forming of a type-II Dirac cone, while the other electron pockets do not.

Quantum oscillation is an important experimental tool to study the electronic properties of materials. As shown in Figs. 3(a) and 3(d), we measured the isothermal magnetization of $PtTe_2$ up to 14 T in $B//c$ and $B//ab$ orientations at various temperatures. Both the out-of-plane ($B//c$) and in-plane ($B//ab$) isothermal magnetizations curves exhibit remarkable dHvA quantum oscillations at low temperature starting from 2.1 and 3.5 T, respectively, indicating a three-dimensional character of the FS. The different background for out-of-plane and in-plane magnetization can be ascribed to the difference of sample holders used for measurements. After subtracting a smooth paramagnetic ($B//c$) or diamagnetic ($B//ab$) background from the measured curves, the periodic oscillations become more clear in $1/B$ up to 25 K as shown in Figs. 3(b) and 3(e). Strong oscillations with the amplitudes of $\sim$15 emu/mol at $T = 2$ K are clearly observed for $B//c$ which is comparable to that of ZrSiH (H = Se and Te) [35]. In the geometry of $B//ab$, $PtTe_2$ show weaker oscillations amplitude as compared to $B//c$. The oscillations pattern for $B//c$ are likely to involve two close frequencies or one dominant frequency, while the quantum oscillations pattern for $B//ab$ seems to involve multiple frequencies, which confirms the conspicuous anisotropy of the FS.

The number and magnitude of all the frequencies involved in quantum oscillation can be derived from its fast Fourier transform (FFT) analysis as shown in Figs. 3(c) and 3(f). For the case of $B//c$, we get two close and strong frequencies $F1 = 102.7$ T, $F2 = 107.8$ T, and a weak frequency $F3 = 243.2$ T from the FFT spectra. The observation of beat ($F1$ and $F2$) means this section is not centered at a high symmetry point in momentum space [36]. $F1$ and $F2$ can also be observed in another sample (see the Supplemental Material [37]). The frequency around 207.2 T should be a second harmonic peak of $F1$. These frequencies observed in FFT spectra are closely related with the orthogonal extremal cross-sectional area (A_F) of the Fermi pockets by the Onsager relation $F = (\Phi_0/2\pi^2)A_F$, where $\Phi_0 = h/2e$ is the magnetic flux quantum. According to the formula, A_F corresponding to $F1$, $F2$, and $F3$ are $A_{F1} = 98.0\times10^{-4}$ Å^{-2}, $A_{F2} = 102.9\times10^{-4}$ Å^{-2}, and $A_{F3} = 232.2\times10^{-4}$ Å^{-2}, occupying 0.35%, 0.37%, and 0.82% of the cross-sectional area of the first BZ in the ab plane, respectively. For the case of $B//ab$, we get $F4 = 148.9$ T, $F5 = 206.2$ T, $F6 = 225.3$ T, and $F7 \approx 4510$ T from the FFT analysis. A slightly different background subtraction will not affect the frequency and amplitude of ultrahigh frequency $F7$ (see the Supplemental Material [37]). A_F corresponding to $F4$, $F5$, $F6$, and $F7$ are $A_{F4} = 142.1\times10^{-4}$ Å^{-2}, $A_{F5} = 196.8\times10^{-4}$ Å^{-2}, $A_{F6} = 215.1\times10^{-4}$ Å^{-2}, and $A_{F7} = 4305\times10^{-4}$ Å^{-2}, occupying 0.57%, 0.78%, 0.86%, and 17% of the cross-sectional area of the first BZ in the bc plane, respectively. The observation of multiple frequencies in the in-plane quantum oscillations proves the complexity of the band structure of $PtTe_2$, consistent with the first-principles calculations shown above.

To determine the contributing pocket of each quantum oscillation mode, we calculate possible extremal cross-sectional area of electron and hole pockets perpendicular to the direction of the magnetic field. According to our calculation, the frequencies $F1 = 102.7$ T, $F2 = 107.8$ T for $B//c$ correspond to the maximum cross section of fingerlike electron pockets β_2, while $F3 = 243.2$ T comes from the electron pocket γ located around the K point. For the case of $B//ab$, $F4 = 148.9$ T can be ascribed to the electron pocket γ, while $F5 = 206.2$ T and $F6 = 225.3$ T come from the branches of the flowerlike electron pocket β_1. What is more, the highest frequency $F7 \approx 4510$ T originates from the hole pocket α, which is related to the formation of the type-II Dirac cone.

The dHvA quantum oscillation of 3D Dirac system can be described by Lifshitz-Kosevich (LK) formula [38,39], which takes the Berry phase into account [40]:

$$\Delta M \propto -B^{0.5} R_T R_D R_S \sin\left[2\pi\left(\frac{F}{B} - \gamma - \delta\right)\right], \quad (1)$$

where $R_T = (\alpha T m^*/B)/[\sinh(\alpha T m^*/B)]$, $R_D = \exp(-\alpha T_D m^*/B)$, and $R_S = \cos(\pi g m^*/2m_e)$. m^* and m_e is the effective cyclotron mass and free electron mass, respectively. T_D is the Dingle temperature and $\alpha = 2\pi^2 k_B/e\hbar$ is a constant. R_T and R_D derive from the broadening in Landau levels induced by temperature effect in Fermi-Dirac

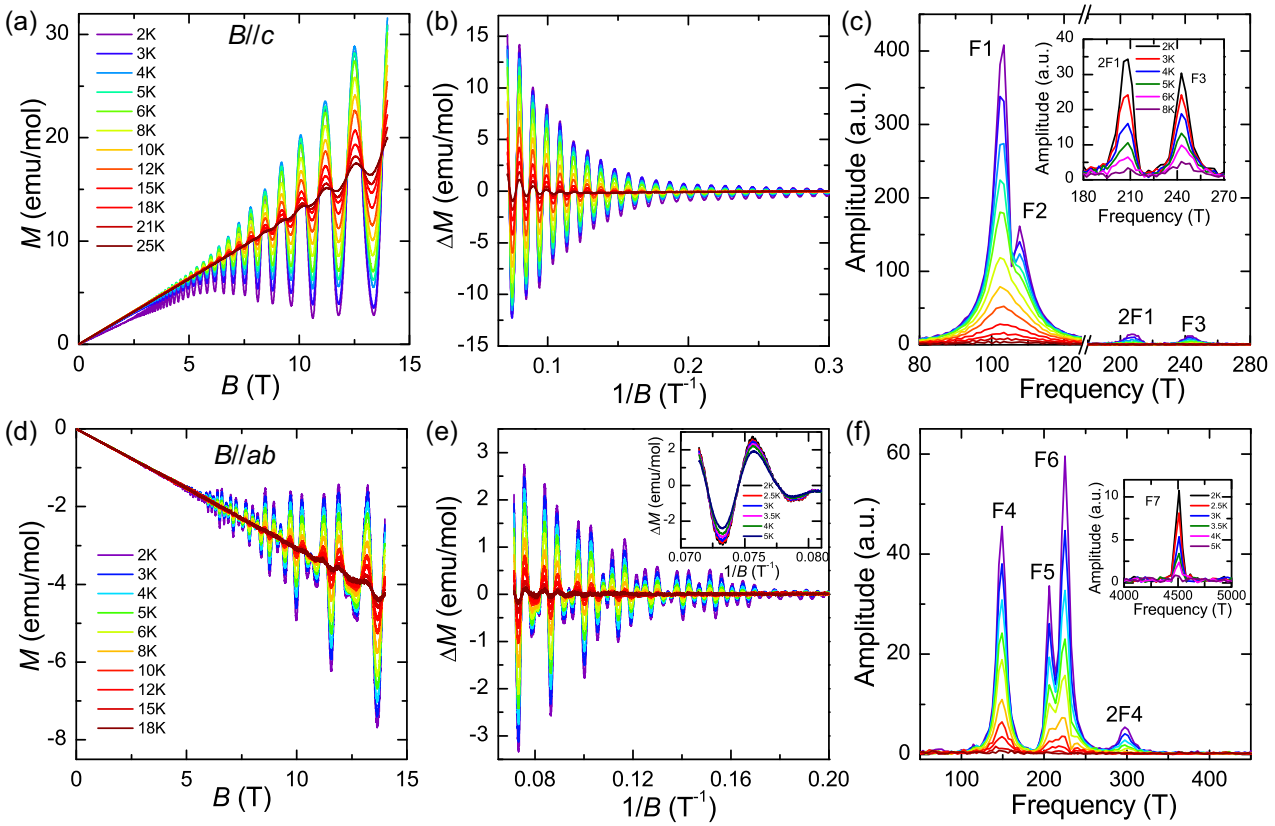

FIG. 3. (a) and (d) Isothermal out-of-plane magnetization and in-plane ($B//[10\bar{1}0]$) magnetization for $PtTe_2$ at various temperatures. (b) and (e) The oscillatory components of the (a) out-of-plane and (d) in-plane magnetization for $PtTe_2$. The inset of (e) shows the enlarged high field data of in-plane oscillatory components. (c) and (f) The FFT spectra of the (b) out-of-plane and (e) in-plane oscillatory components at various temperatures. For (c), the FFT spectra are acquired under field interval $\Delta H = 1$–14 T. The inset shows the FFT spectra of the same oscillatory components under field interval $\Delta H = 2.22$–14 T. For (f), The FFT spectra are acquired under field interval $\Delta H = 3$–14 T. The inset shows the FFT spectra of the same oscillatory components under field interval $\Delta H = 10$–14 T. An ultrahigh frequency around 4500 T is clearly observed.

distribution and electron scattering, respectively. R_T describes the temperature dependence of the oscillation amplitude, while R_D captures the field dependent damping of the oscillation amplitude. What is more, the periodic oscillation of ΔM is depicted by the sine function term with a phase factor $-\gamma - \delta$, where $\gamma = \frac{1}{2} - \frac{\phi_B}{2\pi}$ and ϕ_B is the Berry phase. The dimensionality of FS determines the phase shift δ, specifically $\delta = 0$ and $\pm 1/8$, for the 2D and 3D cases, respectively.

Through the fit of the temperature dependence of the FFT amplitude to the thermal damping factor R_T, we obtain the effective mass of different frequencies as shown in Figs. 4(a) and 4(c). The effective mass for all the observed frequencies are in the range of 0.151 to 0.907 m_e, most of which (except m^* for $F7$) are comparable to that of another kind of type-II DSM $PdTe_2$ [31]. The average m^* for $B//c$ is lower than that for $B//ab$, which originates from the anisotropy of the band structure. For quantum oscillation involving multiple frequencies, it is difficult to get the Dingle temperature of different frequencies by drawing the Dingle plot. However, the Dingle temperature and quantum mobility for every frequency except $F7$ can be extracted by fitting the oscillation patterns at a given temperature ($T = 2$ K) to the multiband LK formula for the 3D case [35]. Multiband LK formula can be considered as the linear superposition of LK formula for a single band, and this approach has been proved to be valid for extracting the transport parameters from quantum oscillations of multiband topological semimetals in previous work [31,35]. As shown in Figs. 4(b) and 4(d), the ΔM for both $B//c$ and $B//ab$ can be precisely reproduced by multiband LK formula and all the parameters determined form the fit are summarized in Table I,

TABLE I. The derived parameters from dHvA oscillations for $PtTe_2$. F is the oscillation frequency, A_F is the extremal cross-sectional area of the pockets, T_D is the Dingle temperature, $m*$ (in terms of m_e) is the effective mass, τ is quantum relaxation time, and μ_q is quantum mobility.

	F (T)	A_F (10^{-4}Å^{-2})	T_D (K)	m^*/m_e	τ (ps)	μ_q (cm^2/Vs)
$B//c$	102.7	98.0	4.3	0.196	0.28	9642
	107.8	102.9	9.5	0.151	0.13	6007
	243.2	232.2	4.2	0.289	0.29	3754
$B//ab$	148.9	142.1	6.8	0.255	0.18	1238
	206.2	196.8	2.8	0.318	0.44	2443
	225.3	215.1	4.2	0.337	0.29	1523
	4510	4305		0.907		

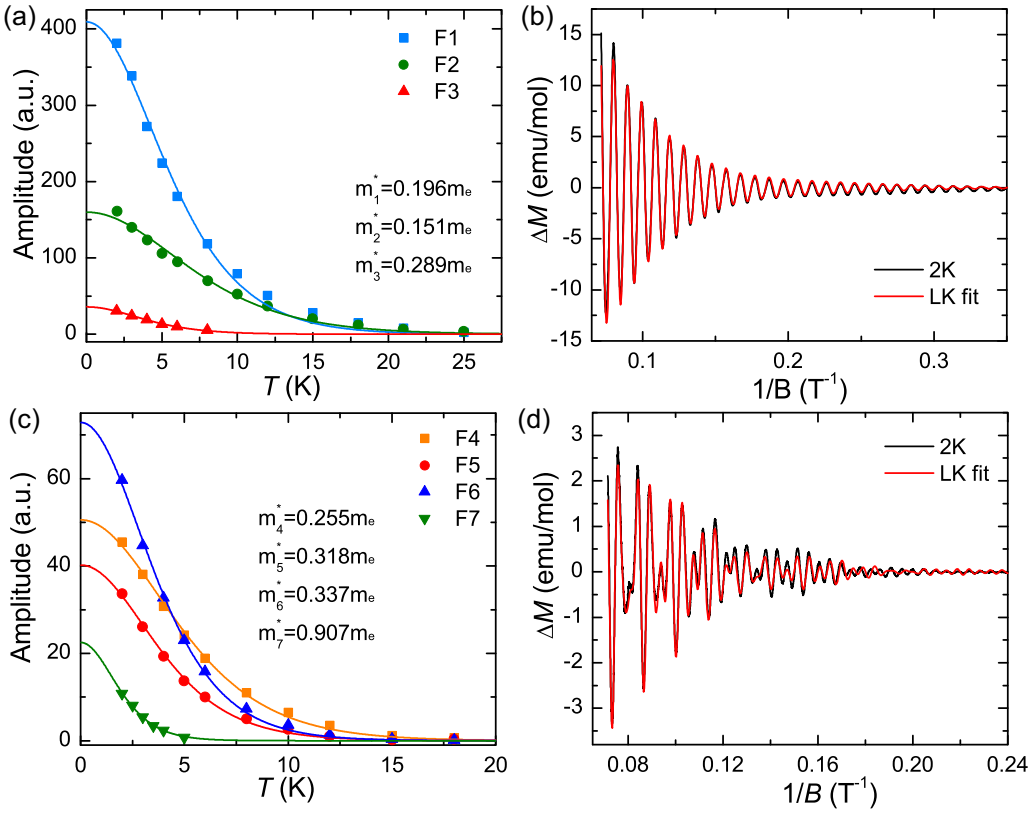

FIG. 4. (a) and (c) Temperature dependence of out-of-plane ($B//c$) and in-plane ($B//ab$) FFT amplitude; the solid lines represent the LK fit for effective mass. The results of the fit are shown in (a) and (c). (b) and (d) The multiband LK fit (red line) of the out-of-plane and in-plane oscillation patterns (black line) at $T = 2$ K.

in which quantum relaxation time and quantum mobility are obtained by $\tau = \hbar/2\pi k_B T_D$ and $\mu = e\tau/m^*$, respectively. The Dingle temperature is determined to be from 2.8 to 9.5 K, and corresponding quantum relaxation time is from 0.13 to 0.44 ps. Furthermore, the quantum mobility for $B//c$ is estimated to be from 3754 to 9642 cm^2/V s, while that for $B//ab$ is calculated to be from 1238 to 2443 cm^2/V s. Obviously the quantum mobility for in-plane cyclotron motions ($B//c$) is much larger than that for out-of-plane cyclotron motions ($B//ab$). The layered structure of $PtTe_2$ may explain such anisotropic quantum mobility. The higher scattering rate along the interlayer direction is likely responsible for the suppression of quantum mobility for $B//ab$. The difference in the amplitude of the dHvA oscillations between the in-plane and out-of-plane directions may be induced by the difference of the quantum mobility and the effective mass between the two directions. Furthermore, it is worth mentioning that the in-plane cyclotron motion quantum mobility for $PtTe_2$ is significantly higher than that for $PdTe_2$. The low effective mass and high quantum mobility hint at the superior transport properties of type-II Dirac semimetal $PtTe_2$.

The angle dependence of dHvA provides further insight into the shape of the FS. The FFT spectra of the dHvA oscillations with field rotated in the ab plane are presented in Fig. 5(a). The FFT peaks can be generally divided into two groups, one group around 130 T, and another group around 210 T. Split peaks and small peaks around $F5$ might be due to strong spin-orbit coupling or complicated FS of flowerlike electron pocket β_1 [41]. The angles dependent positions of two main FFT peaks are summarized in Fig. 5(b). Both $F4$ and $F5$ evolve with the direction of magnetic field with a period of 60° in the ab plane, which is consistent with threefold rotation symmetry of the FS. When the angle θ deviates from 0°, $F4$ increase gradually, and reach maximum value around 148.9 T at $\theta = 30°$. When θ changes from 30° to 60°, $F4$ will approach minimum value again at $\theta = 60°$ around 124 T. This can be explained by the double-triangular-pyramid-like electron pocket γ. We present the FFT spectra of the same oscillatory components under field interval $\Delta H = 10$–14 T in Fig. 5(c). The highest frequency appears only when the magnetic field is along or near Γ-M direction in the BZ. The strange property of the highest frequency may arise from the angular dependence of the minimum orthogonal cross-sectional area for the hole pocket α, which take the lowest value when the magnetic field is along Γ-M direction. If the magnetic field deviates from Γ-M direction, the minimum orthogonal cross-sectional area will increase, which make it more difficult to detect the ultrahigh frequency above 4000 T. Therefore, the hole pocket α in the center of BZ shows strong anisotropy. The FS measured by dHvA is consistent with the theoretical calculation, providing indirect evidence for the existence of tilted Dirac cones in $PtTe_2$.

IV. CONCLUSIONS

In summary, we study the magnetic transport properties and band structure of type-II DSM $PtTe_2$ by dHvA quantum

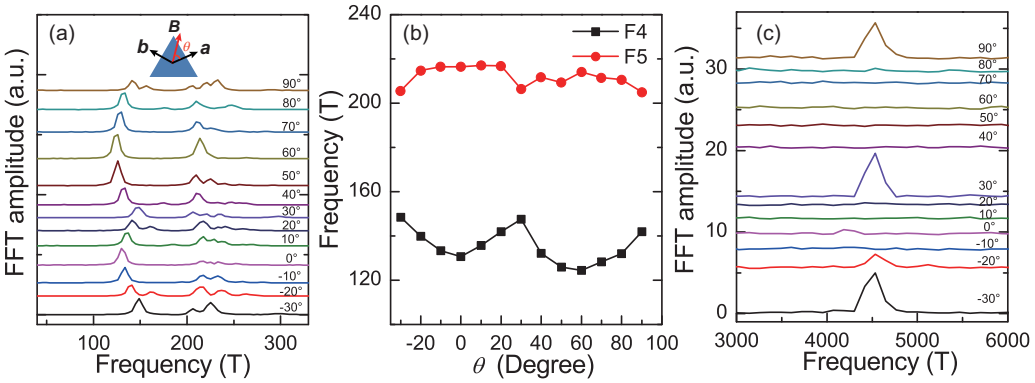

FIG. 5. (a) FFT spectra of the dHvA quantum oscillations with field rotated in the *ab* plane. Inset in (a) shows the definition of field orientation angle θ. The data collected at different θ have been shifted vertically for clarity. (b) The angular dependencies of the main oscillation frequencies obtained from (a). (c) The FFT spectra of the same oscillatory components under field interval $\Delta H = 10$–14 T.

oscillations. Strong oscillations are observed for both the out-of-plane and in-plane isothermal magnetization in low temperature. Multiple frequencies are extracted from the oscillations and analyzed based on the Lifshitz-Kosevich (LK) formula. The low effective mass for most frequencies is comparable to that of another kind of type-II Dirac semimetal $PdTe_2$, while the average mobility for most frequencies is significantly higher than that of $PdTe_2$ [31]. Angle dependent in-plane dHvA oscillations provide further insights into FS properties. In addition, the first-principles calculations are conducted to help us verify the topological nature and identify the contributing pocket of each frequency. Especially the ultrahigh frequency around 4510 T is considered to result from the electron pocket that contributes to the formation of the type-II Dirac cone.

ACKNOWLEDGMENTS

We gratefully acknowledge the financial support of the National Key R&D Program of China (2017YFA0303203), the National Natural Science Foundation of China (U1732273, U1732159, 91421109, 91622115, 11522432, and 11574217), the Fundamental Research Funds for the Central Universities (14380091, 14380082), the NSF of Jiangsu Province (Grant BK20160659), and the opening Project of Wuhan National High Magnetic Field Center. We would also like to acknowledge the assistance of the Nanofabrication and Characterization Center at the Physics College of Nanjing University. We also thank Professor Haihu Wen, Associate Professor Xiyu Zhu, and Dr. Hai Lin in Nanjing University, China for help with Laue diffraction pattern measurements.

D. Fu, X. Bo, and F. Fei contributed equally to this work.

[1] H. Weyl, Proc. Natl. Acad. Sci. USA **15**, 323 (1929).

[2] S.-Y. Xu, I. Belopolski, N. Alidoust, M. Neupane, G. Bian, C. Zhang, R. Sankar, G. Chang, Z. Yuan, C.-C. Lee, S.-M. Huang, H. Zheng, J. Ma, D. S. Sanchez, B. Wang, A. Bansil, F. Chou, P. P. Shibayev, H. Lin, S. Jia, and M. Z. Hasan, Science **349**, 613 (2015).

[3] B. Q. Lv, H. M. Weng, B. B. Fu, X. P. Wang, H. Miao, J. Ma, P. Richard, X. C. Huang, L. X. Zhao, G. F. Chen, Z. Fang, X. Dai, T. Qian, and H. Ding, Phys. Rev. X **5**, 031013 (2015).

[4] X.-C. Pan, X. Chen, H. Liu, Y. Feng, Z. Wei, Y. Zhou, Z. Chi, L. Pi, F. Yen, F. Song, X. Wan, Z. Yang, B. Wang, G. Wang, and Y. Zhang, Nat. Commun. **6**, 7805 (2015).

[5] L. He, Y. Jia, S. Zhang, X. Hong, C. Jin, and S. Li, npj Quantum Mater. **1**, 16014 (2016).

[6] Y. Du, F. Tang, D. Wang, L. Sheng, E.-j. Kan, C.-G. Duan, S. Y. Savrasov, and X. Wan, npj Quantum Mater. **2**, 3 (2017).

[7] D. Fu, B. Zhang, X. Pan, F. Fei, Y. Chen, M. Gao, S. Wu, J. He, Z. Bai, Y. Pan, Q. Zhang, X. Wang, X. Wu, and F. Song, Sci. Rep. **7**, 12688 (2017).

[8] F. Dongzhi, P. Xingchen, B. Zhanbin, F. Fucong, A. U.-M. Gilberto, S. Honglian, W. Xuelin, W. Baigeng, and S. Fengqi, Nanotechnology **29**, 135705 (2018).

[9] Z. K. Liu, B. Zhou, Y. Zhang, Z. J. Wang, H. M. Weng, D. Prabhakaran, S.-K. Mo, Z. X. Shen, Z. Fang, X. Dai, Z. Hussain, and Y. L. Chen, Science **343**, 864 (2014).

[10] J. Xiong, S. K. Kushwaha, T. Liang, J. W. Krizan, M. Hirschberger, W. Wang, R. J. Cava, and N. P. Ong, Science **350**, 413 (2015).

[11] M. Neupane, S.-Y. Xu, R. Sankar, N. Alidoust, G. Bian, C. Liu, I. Belopolski, T.-R. Chang, H.-T. Jeng, H. Lin, A. Bansil, F. Chou, and M. Z. Hasan, Nat. Commun. **5**, 3786 (2014).

[12] Z. K. Liu, J. Jiang, B. Zhou, Z. J. Wang, Y. Zhang, H. M. Weng, D. Prabhakaran, S. K. Mo, H. Peng, P. Dudin, T. Kim, M. Hoesch, Z. Fang, X. Dai, Z. X. Shen, D. L. Feng, Z. Hussain, and Y. L. Chen, Nat. Mater. **13**, 677 (2014).

[13] L. X. Yang, Z. K. Liu, Y. Sun, H. Peng, H. F. Yang, T. Zhang, B. Zhou, Y. Zhang, Y. F. Guo, M. Rahn, D. Prabhakaran, Z. Hussain, S. K. Mo, C. Felser, B. Yan, and Y. L. Chen, Nat. Phys. **11**, 728 (2015).

[14] X. Huang, L. Zhao, Y. Long, P. Wang, D. Chen, Z. Yang, H. Liang, M. Xue, H. Weng, Z. Fang, X. Dai, and G. Chen, Phys. Rev. X **5**, 031023 (2015).

[15] C.-L. Zhang, S.-Y. Xu, I. Belopolski, Z. Yuan, Z. Lin, B. Tong, G. Bian, N. Alidoust, C.-C. Lee, S.-M. Huang, T.-R. Chang, G. Chang, C.-H. Hsu, H.-T. Jeng, M. Neupane, D. S. Sanchez, H. Zheng, J. Wang, H. Lin, C. Zhang, H.-Z. Lu, S.-Q. Shen, T. Neupert, M. Z. Hasan, and S. Jia, Nat. Commun. **7**, 10735 (2016).

[16] A. C. Potter, I. Kimchi, and A. Vishwanath, Nat. Commun. **5**, 5161 (2014).

[17] P. J. W. Moll, N. L. Nair, T. Helm, A. C. Potter, I. Kimchi, A. Vishwanath, and J. G. Analytis, Nature (London) **535**, 266 (2016).
[18] A. A. Soluyanov, D. Gresch, Z. Wang, Q. Wu, M. Troyer, X. Dai, and B. A. Bernevig, Nature (London) **527**, 495 (2015).
[19] P. Li, Y. Wen, X. He, Q. Zhang, C. Xia, Z.-M. Yu, S. A. Yang, Z. Zhu, H. N. Alshareef, and X.-X. Zhang, Nat. Commun. **8**, 2150 (2017).
[20] Z. Wang, D. Gresch, A. A. Soluyanov, W. Xie, S. Kushwaha, X. Dai, M. Troyer, R. J. Cava, and B. A. Bernevig, Phys. Rev. Lett. **117**, 056805 (2016).
[21] L. Huang, T. M. McCormick, M. Ochi, Z. Zhao, M.-T. Suzuki, R. Arita, Y. Wu, D. Mou, H. Cao, J. Yan, N. Trivedi, and A. Kaminski, Nat. Mater. **15**, 1155 (2016).
[22] T.-R. Chang, S.-Y. Xu, G. Chang, C.-C. Lee, S.-M. Huang, B. Wang, G. Bian, H. Zheng, D. S. Sanchez, I. Belopolski, N. Alidoust, M. Neupane, A. Bansil, H.-T. Jeng, H. Lin, and M. Z. Hasan, Nat. Commun. **7**, 10639 (2016).
[23] I. Belopolski, D. S. Sanchez, Y. Ishida, X. Pan, P. Yu, S.-Y. Xu, G. Chang, T.-R. Chang, H. Zheng, N. Alidoust, G. Bian, M. Neupane, S.-M. Huang, C.-C. Lee, Y. Song, H. Bu, G. Wang, S. Li, G. Eda, H.-T. Jeng, T. Kondo, H. Lin, Z. Liu, F. Song, S. Shin, and M. Z. Hasan, Nat. Commun. **7**, 13643 (2016).
[24] S.-Y. Xu, N. Alidoust, G. Chang, H. Lu, B. Singh, I. Belopolski, D. S. Sanchez, X. Zhang, G. Bian, H. Zheng, M.-A. Husanu, Y. Bian, S.-M. Huang, C.-H. Hsu, T.-R. Chang, H.-T. Jeng, A. Bansil, T. Neupert, V. N. Strocov, H. Lin, S. Jia, and M. Z. Hasan, Sci. Adv. **3**, e1603266 (2017).
[25] M. Udagawa and E. J. Bergholtz, Phys. Rev. Lett. **117**, 086401 (2016).
[26] A. A. Zyuzin and R. P. Tiwari, JETP Lett. **103**, 717 (2016).
[27] T. E. O'Brien, M. Diez, and C. W. J. Beenakker, Phys. Rev. Lett. **116**, 236401 (2016).
[28] H. Huang, S. Zhou, and W. Duan, Phys. Rev. B **94**, 121117 (2016).
[29] M. Yan, H. Huang, K. Zhang, E. Wang, W. Yao, K. Deng, G. Wan, H. Zhang, M. Arita, H. Yang, Z. Sun, H. Yao, Y. Wu, S. Fan, W. Duan, and S. Zhou, Nat. Commun. **8**, 257 (2017).
[30] K. Zhang, M. Yan, H. Zhang, H. Huang, M. Arita, Z. Sun, W. Duan, Y. Wu, and S. Zhou, Phys. Rev. B **96**, 125102 (2017).
[31] F. Fei, X. Bo, R. Wang, B. Wu, J. Jiang, D. Fu, M. Gao, H. Zheng, Y. Chen, X. Wang, H. Bu, F. Song, X. Wan, B. Wang, and G. Wang, Phys. Rev. B **96**, 041201 (2017).
[32] T.-R. Chang, S.-Y. Xu, D. S. Sanchez, W.-F. Tsai, S.-M. Huang, G. Chang, C.-H. Hsu, G. Bian, I. Belopolski, Z.-M. Yu, S. A. Yang, T. Neupert, H.-T. Jeng, H. Lin, and M. Z. Hasan, Phys. Rev. Lett. **119**, 026404 (2017).
[33] H.-J. Noh, J. Jeong, E.-J. Cho, K. Kim, B. I. Min, and B.-G. Park, Phys. Rev. Lett. **119**, 016401 (2017).
[34] A. Glamazda, K. Y. Choi, P. Lemmens, J. J. Yang, and S. W. Cheong, New J. Phys. **16**, 093061 (2014).
[35] J. Hu, Z. Tang, J. Liu, X. Liu, Y. Zhu, D. Graf, K. Myhro, S. Tran, C. N. Lau, J. Wei, and Z. Mao, Phys. Rev. Lett. **117**, 016602 (2016).
[36] A. E. Dunsworth, J. Low Temp. Phys. **19**, 51 (1975).
[37] See Supplemental Material at http://link.aps.org/supplemental/10.1103/PhysRevB.97.245109 for details on confirmation for the general reproducibility of $F1$, $F2$ in $PtTe_2$ and analysis for the effect of different background subtraction on frequency and amplitude of all the oscillation modes.
[38] I. M. Lifshitz and A. M. Kosevich, Sov. Phys. JETP **2**, 636 (1956).
[39] D. Shoenberg, *Magnetic Oscillations in Metals* (Cambridge University Press, Cambridge, 1984).
[40] G. P. Mikitik and Y. V. Sharlai, Phys. Rev. Lett. **82**, 2147 (1999).
[41] A. Wang, D. Graf, A. Stein, Y. Liu, W. Yin, and C. Petrovic, Phys. Rev. B **96**, 195107 (2017).